Quaternary Science Reviews 89 (2014) 94–107

Contents lists available at ScienceDirect

Quaternary Science Reviews

journal homepage: www.elsevier.com/locate/quascirev

Towards successful OSL sampling strategies in glacial environments: deciphering the influence of depositional processes on bleaching of modern glacial sediments from Jostedalen, Southern Norway

G.E. King*, R.A.J. Robinson, A.A. Finch

Department of Earth and Environmental Sciences, University of St Andrews, Irvine Building, North Street, St Andrews, Fife KY16 9AL, Scotland, UK

ARTICLE INFO

Article history:
Received 8 November 2013
Received in revised form
27 January 2014
Accepted 4 February 2014
Available online

Keywords:
Optically stimulated luminescence dating
Glacial sediments
Transport and depositional processes
Partial bleaching

ABSTRACT

The optically stimulated luminescence (OSL) signals of quartz and K-feldspar are known to bleach poorly within some glacial settings, and can present a major challenge to dating applications. However, because the OSL signal is extremely sensitive to sunlight exposure history, the residual luminescence signals of modern glacial sediments also encode information about transport and depositional processes. Through examination of the residual luminescence properties (equivalent dose (D_e) and overdispersion values) of a suite of modern glacial sediments from different depositional settings (sandar, proglacial delta and main meltwater channel), this study provides insights not only into which sediments are likely to be fully bleached within glacial settings, but also into how OSL can be used to trace different depositional processes across sedimentary landforms. Improved understanding of the processes of sediment bleaching will enable better sample selection and may improve the accuracy and precision of OSL dating of glacial sediments.

The luminescence signals of both coarse-grained quartz and K-feldspar with similar sediment sources are found to be sensitive to both depositional process and specific depositional setting. Whereas modern braid-bar-head deposits from the Nigardsdalen ice-proximal proglacial delta typically have ages of $\leq$3 ka, similar depositional features from the Fåbergstølsgrandane sandur have residual ages of $\geq$26 ka. Exploration of changing residual luminescence signals across individual sandur and proglacial delta braid-bar features shows that braid-bar-head deposits can retain large residual D_e values, while the partner braid-bar-tail deposits are almost completely bleached. The quartz OSL signal and K-feldspar $IRSL_{50}$ and post-IR $IRSL_{250}$ signals are shown to bleach at the same rate across the same bar feature and the $IRSL_{50}$ K-feldspar signal is also shown to be completely bleached for bar-tail deposits in Nigardsdalen. Therefore the $IRSL_{50}$ K-feldspar signal is suitable for dating some glacial deposits, circumventing the challenges associated with dim quartz signals.

1. Introduction

Optically stimulated luminescence (OSL) dating is one of the favoured methods for dating glacial sediments, however partial resetting (bleaching) of luminescence signals can present a major challenge within glacial environments (e.g. Gemmell, 1988; Mejdahl and Funder, 1994). Although there has been considerable research on quantifying the unbleached residuals in glacial settings (e.g. Alexanderson and Murray, 2012a) and how to ameliorate and/or avoid these effects (e.g. Fuchs and Owen, 2008), little research has explored the processes of sediment bleaching. Stokes et al. (2001) explored differential bleaching of fluvial sediments with increasing transport distances in large continental scale drainage basins, and Ditlefsen (1992) and Klasen et al. (2006, 2007) explored the rates of sediment bleaching for different grain sizes in laboratory based studies. King et al. (2013) recorded unbleached residual signals of 0–3 ka for glaciofluvial bar deposits 2 km from the ice-margin, but were unable to identify a single cause for the residual variability, attributing it to a combination of specific depositional setting, sediment source and transport distance. If the causes of unbleached residual luminescence signals can be well constrained it may be possible to exploit changing residual signals in the exploration of depositional pathway tracing.

* Corresponding author. Present address: Institute of Earth Surface Dynamics, University of Lausanne, Quartier UNIL-Mouline, Bâtiment Géopolis, 1015 Lausanne, Switzerland.
E-mail addresses: georgina.king@gmail.com, georgina.king@unil.ch (G.E. King).

http://dx.doi.org/10.1016/j.quascirev.2014.02.001

This study explores the causes of variability in residual luminescence signals from depositional features through measuring the luminescence properties of multiple sediments from individual landforms. Sampling in such high resolution enables the signatures of the specific depositional processes to be isolated from the varying influences of sediment transport distance and source material which can fluctuate at the catchment scale. Two main glacial catchments have been investigated which comprise a proglacial delta and sandur, both of which are characterised by braid-bar deposits with varying spatial scales. Sandur braid-bar deposits are considered favourable for luminescence dating (see Thrasher et al., 2009a for a review), and it is therefore important that the processes of sediment bleaching are understood. Understanding variations in residual luminescence signals and by inference the bleaching properties of different deposits will not only enable exploration of depositional pathway tracing but will also enable more informed OSL sample selection in both glaciofluvial and fluvial depositional settings.

2. Partial bleaching in glacial settings

In glacial environments the degree of sediment bleaching varies between different deposits, encoding information about transport and depositional processes. Partial bleaching is thought to affect sediments most where they are transported rapidly, and over short distances, such as in a turbulent meltwater flow (e.g. Ditlefsen, 1992; Rhodes and Pownall, 1994). In contrast some sedimentary features in glacial and fluvial depositional environments have been identified which are thought to be less susceptible to partial bleaching effects (e.g. Murray et al., 1995; Preusser, 1999; Robinson et al., 2005; Fuchs and Owen, 2008; Thrasher et al., 2009b). For example, whereas the head of a braid-bar essentially comprises channel material and is poorly bleached; the sediments that accrete on the bar-tops following periods of elevated discharge experience greater opportunities for sediment bleaching, and material at the bar-tails which has been either transported across the bar-features or alongside them, potentially experiences the greatest sunlight exposure and may be fully reset. Channel bars are also emergent for part of the discharge cycle, and material is reworked over the bar tops episodically, influencing sediment bleaching opportunities. Sediment facies can be used to infer depositional context and process, and probable light exposure history (Fuchs and Owen, 2008; Thrasher et al., 2009a).

2.1. Identifying and characterising partially reset OSL signals

Duller (1994) describes two types of partially reset sediments. Type 'A' sediments are those that have been homogeneously, but incompletely bleached, whereas type 'B' sediments have been heterogeneously partially bleached. The occurrence of type 'A' sediments is thought to be unlikely in most natural depositional settings (Duller, 2008), and partially reset OSL signals can generally be identified through examination of the distribution of equivalent dose (D_e) values measured when a sample is dated using OSL (e.g. Arnold et al., 2007, Fig. 1). This is because partially bleached (type 'B') sediments exhibit greater scatter (overdispersion) in D_e values than completely bleached sediments. Sample overdispersion is calculated from the distribution of D_e values and is the relative standard deviation of all D_e values, once uncertainties have been incorporated (Galbraith et al., 1999). Even fully bleached (reset) samples exhibit overdispersion and it has various causes in addition to heterogeneous bleaching (e.g. Murray et al., 1995), including post-depositional mixing of sediments of different depositional ages (e.g. Bateman et al., 2007), beta dose-rate heterogeneity (e.g. Nathan et al., 2003) and variable responses of different grains to fixed measurement conditions. When multi-grain aliquots, rather than single-grains are analysed, the effects of beta-dose rate heterogeneity are mediated, and heterogeneous bleaching and post-depositional mixing of sediments are the most significant drivers of sample overdispersion. Galbraith et al. (1999) have proposed that samples with overdispersion values of <20% are homogenously bleached and in their more recent review, Arnold and Roberts (2009) report an average value of 13 ± 7% overdispersion for samples from the published literature that are thought to be homogeneously bleached and have been measured using multi-grain aliquots. King et al. (2013) recently demonstrated that from a set of modern subglacial, paraglacial and glaciofluvial bar deposits, some of the most (albeit incompletely) bleached samples exhibited the highest overdispersion values. Thus sample overdispersion encodes further information about the bleaching and transport and depositional process history of sediments, when considered relative to their residual dose and depositional context. Through measuring the residual luminescence signals of multiple samples from specific positions on braid-bar deposits, this research will provide a greater understanding of the controls that sedimentary processes have on the OSL signals of quartz and K-feldspar.

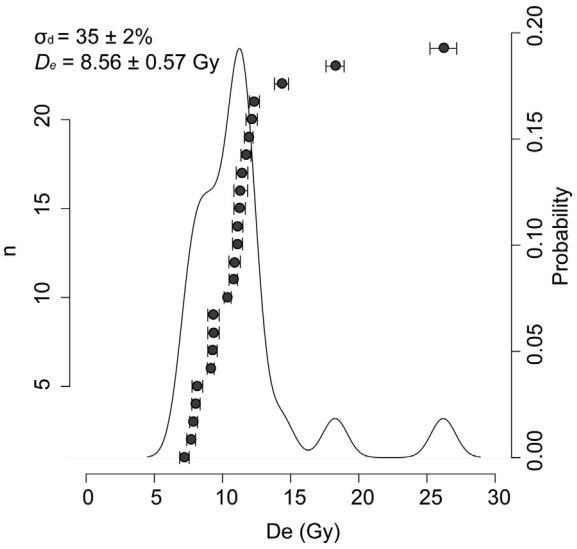

Fig. 1. Kernel density estimate of the K-feldspar extract of GRAN57. Plot drawn in RStudio (2012) using the gplots (Warnes et al., 2010) and plotrix packages (Lemon et al., 2012).

3. Study area

A suite of outlet-glacier catchments which drain the Jostedalsbreen ice-cap in Southern Norway were selected as the sample sites, as they comprise a range of glaciofluvial depositional environments. Three catchments have been specifically explored in this research: Stordalen, Fåbergstølsgrandane and Nigardsdalen (Fig. 2). Stordalen is a narrow catchment, dominated by a single meltwater channel that drains Lodalsbreen; Fåbergstølsgrandane is a sandur and Nigardsbreen drains into a proglacial lake where a delta has formed.

The Jostedalsbre Plateau is thought to have been completely ice free 7.5–5.5 ka cal BP (Nesje and Kvamme, 1991; Matthews et al., 2000; Nesje et al., 2000, 2001), and the various valleys containing outlet glaciers to have been fully deglaciated by ~8 ka BP (Nesje et al., 1991; original 9 ka BP age calibrated using IntCal09 (Reimer et al., 2009) assuming an uncertainty of 100 years in OxCal v.4.2 (Bronk Ramsey, 2013)). Jostedalen experienced Neoglaciation from

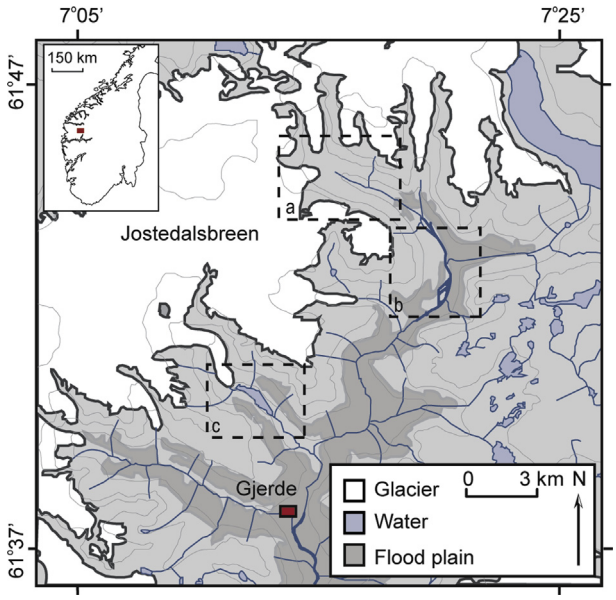

Fig. 2. Map of the study area, inset shows the location of Jostedalen in Southern Norway and boxes show the locations of a) Stordalen, b) Fåbergstølsgrandane and c) Nigardsdalen.

~5 ka BP (Shakesby et al., 2004), and substantial advances occurred between 3.7 and 3.1 ka BP (Ballantyne and Benn, 1994; Ballantyne, 1995). The various outlet glaciers of the Jostedalsbreen ice-cap have multiple retreat moraines, attributed to the LIA which has been the most substantial readvance of the Neoglacial period (Dahl et al., 2002). Nigardsdalen was fully glaciated during the LIA, and in 1822 the Lodalsbreen and Stigaholtsbreen glaciers are known to have advanced onto the margin of Fåbergstølsgrandane from historical records (Nussbaumer et al., 2011).

The geomorphology of this region is characterised by glacial erosion and sediment reworking, which results in paraglacial sedimentation (Church and Ryder, 1972) and debris flows are a common paraglacial process within Jostedalen (e.g. Curry, 1999; Curry and Ballantyne, 1999). The geology of Jostedalen varies from quartz monzanite to quartz diorite. It is within the western Gneiss region of Norway (Bryhni and Sturt, 1985), and is underlain by bedrock of Precambrian granitic to granodioritic gneiss (Holtedahl, 1960; Holtedahl and Dons, 1960).

4. Site and sample descriptions

In this study, glaciofluvial bar tops (horizontally (Sh) and ripple (Sr) bedded sands) and backs (Sh, Sr) were focussed upon during sampling (Fig. 3). Only modern samples have been collected in order that the process signatures, rather than the chronologies of the deposits can be explored; sample modernity was ensured through sampling surface proximal sediments. Furthermore, deglaciation of Jostedalen following the Little Ice Age (LIA) at ~1750 AD means that any *in-situ* deposit from Nigardsdalen or Stordalen must have a maximum age of only ~250 years (Dahl et al., 2002). In addition to sampling a suite of braid-bars, three valley main meltwater channel side-attached bar samples from Stordalen and a sandur main-meltwater channel side-attached bar sample from Fåbergstølsgrandane were also taken. These samples enable the degree of sediment bleaching with increasing transport distances up to 7 km from the ice front to be investigated.

Samples were collected at the start of the melt-season in June 2008. The snow-pack had not completely melted at the time of sampling which initially rendered some sites inaccessible (e.g. Stordalen) although much of the snow melted throughout the four week sampling period. There were two precipitation events with >10 mm of rainfall throughout the sampling period (10th and 11th June 2008) which resulted in elevated discharges, although snowmelt (and precipitation induced snowmelt) was the greatest driver of changing discharge throughout June 2008. Almost 90% of the total discharge from the Jostedøla which drains the study area occurs during the summer months (Odland et al., 1991).

4.1. Stordalen (LOD)

The debris-covered Lodalsbreen glacier occupies the upper region of the Stordalen valley, and the catchment also has direct

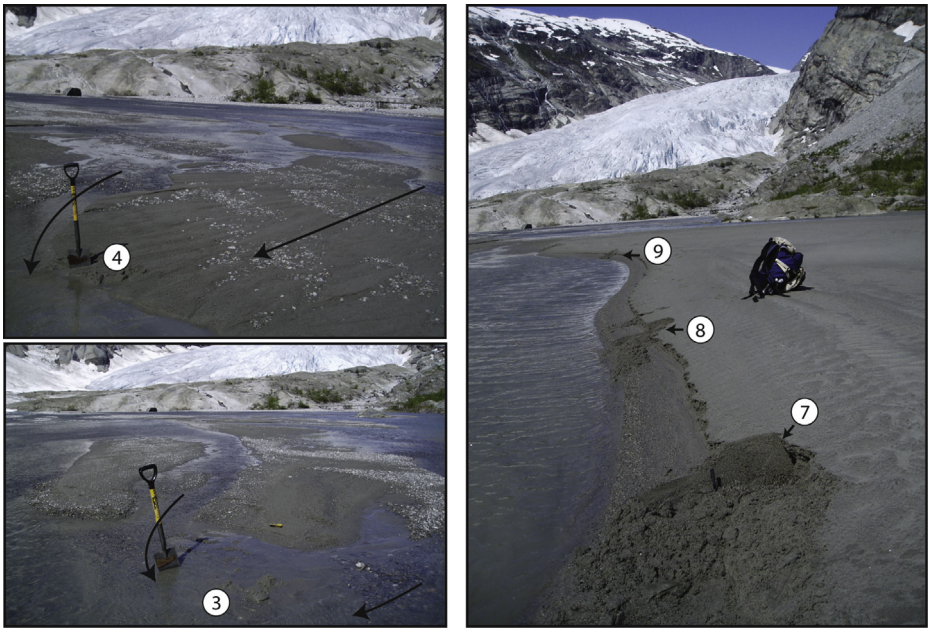

Fig. 3. Photographs of five of the braid-bar deposits sampled from Nigardsdalen. Sample locations of MJO3, MJO4, MJO7, MJO8 and MJO9 are shown.

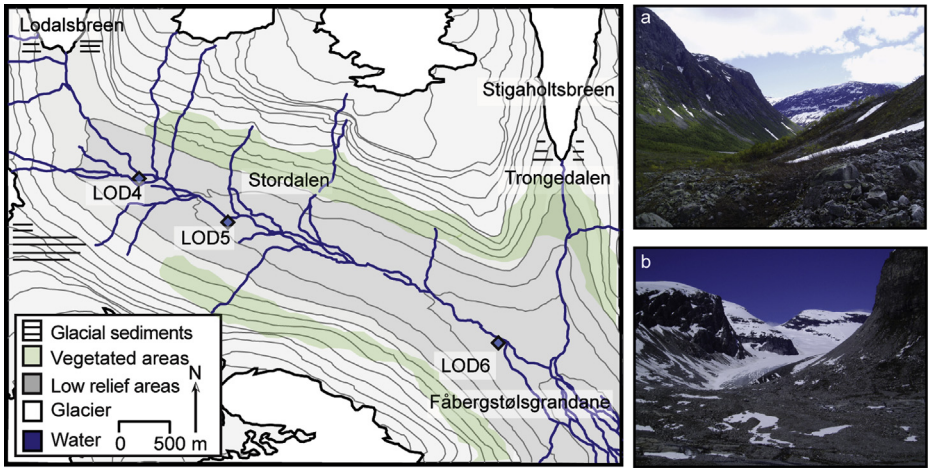

Fig. 4. Map of the Stordalen side-attached bar deposit sample locations. Sample GRAN69 is taken from Fåbergstølsgrandane and is shown in Fig. 5; a) view towards Fåbergstølsgrandane (east) and b) view of Lodalsbreen (north).

glacial inputs from the Jostedalsbreen ice-cap (Fig. 4). There are some paraglacial deposits present in the catchment, although paraglacial material provides a small component of the total sediment input relative to subglacial sediment sources. Three valley main meltwater channel side-attached bars were sampled at increasing distance from the Lodalsbreen glacier along the Stordalen meltwater channel (LOD4 (1.3 km), LOD5 (1.8 km) and LOD6 (4.5 km)) as well as a Fåbergstølsgrandane sandur main meltwater channel side-attached bar (GRAN69 (6.7 km), Fig. 5). The sediment sources for the three Stordalen samples and sample GRAN69 are broadly similar; GRAN69 is partly sourced from Stordalen, but also has subglacial and limited paraglacial sediment inputs from Trongedalen (Fig. 5). As the source sediments are similar the influence of changing transport distances on the residual luminescence properties of sediments transported by the same depositional processes can be explored. These samples are important to characterise the luminescence properties of materials input to Fåbergstølsgrandane. The K-feldspar luminescence signals of these four samples have been measured.

4.2. Fåbergstølsgrandane (GRAN)

The Fåbergstølsgrandane sandur is the largest in Norway (Fig. 5). Sandar comprise a complex facies assemblage both laterally and horizontally reflecting the varied discharge patterns and associated sediment fluxes of glacial environments. Thrasher et al. (2009b) developed a conceptual model which explores the different depositional pathways and environments of a proglacial sandur, and associated facies (Miall, 1985; Brookfield and Martini, 1999; Boyce and Eyles, 2000). The depositional processes that operate on a sandur are similar to braided river channels, although fine grained sediment accumulations on bar tops are rare or absent (Reineck and Singh, 1973). The braided channel bars in Fåbergstølsgrandane range from cobble-gravel bars of ~1 m elevation in the upper catchment, to gravel-coarse-sand bars of ~30 cm elevation in the lower (SE) catchment. Material has been sampled from similar scale features with elevations of ~30 cm and lengths of ~150 m, which are ~200 m from the main meltwater channel. The bars sampled comprise mainly sand, grading into gravel, although some cobbles were also present on the bars.

As the potential sunlight exposure of sediments varies dependent upon their specific location on a braid-bar feature, a suite of bar-head (GRAN54, 58, 59), bar-mid (GRAN55) and bar-tail deposits (GRAN56 and 57) were sampled from an individual bar feature (GRAN54, 55, 56, Fig. 5) and two other bar forms. Both the quartz and K-feldspar luminescence signals were measured.

4.3. Nigardsdalen (MJO)

Nigardsbreen discharges into a proglacial lake which formed following glacial retreat in the 1930s (Østrem et al., 1976). A delta of braid-bars has formed within the lake and the processes of deposition are similar between Nigardsdalen (also known as Mjolverdalen) and Fåbergstølsgrandane, as both catchments have low gradients and comprise anastomosing meltwater channels. However, whereas in Fåbergstølsgrandane the different braided bar features have elevations of ~1 m in the upper catchment, maximum elevations are

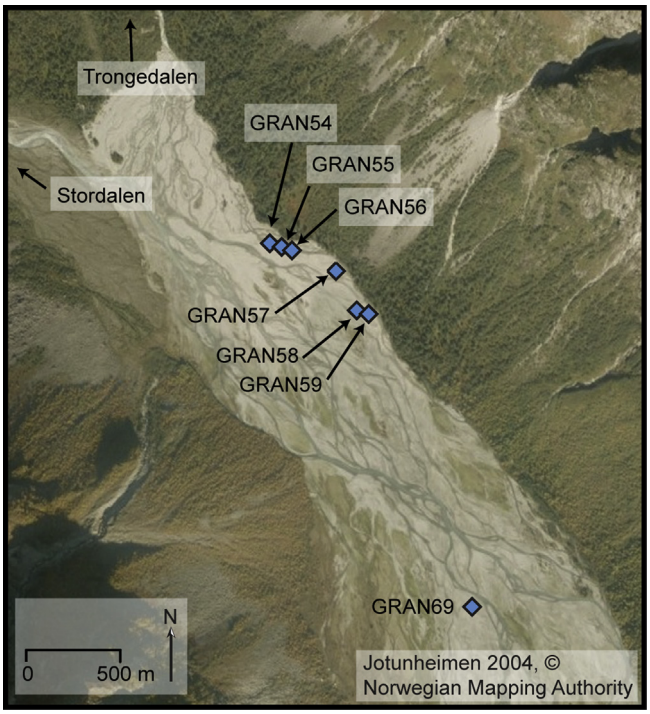

Fig. 5. Aerial photograph of Fåbergstølsgrandane showing the sample locations of the six braid-bar deposits sampled, and side-attached bar sample GRAN69.

~30 cm throughout Nigardsdalen (Fig. 3). Elevation values are approximate and fluctuate throughout the ablation season in response to changing meltwater channel discharge, however Nigardsdalen comprises a shallower system than Fåbergstølsgrandane, within which sediments experience higher frequency reworking across channel bars because of their relatively low relief.

In Nigardsdalen, sediments are sourced predominantly from subglacial material, as only limited paraglacial material is present and two composite braided bar features were sampled from Nigardsdalen at positions ~200 m (Bar 1) and ~300 m (Bar 2) downstream from the glacial snout (Fig. 6). Bar 1 is approximately ~70 m in length, whereas bar 2 is ~50 m in length. The elevation of bar 1 is ~5 cm in comparison to ~30 cm for bar 2. The bars are smaller but similar in scale to the braid-bars sampled from Fåbergstølsgrandane; however whereas pebbles and cobbles were present on the Fåbergstølsgrandane braid-bars, the largest clast size on the Nigardsdalen bars sampled are pebbles. Braid-bar-head (MJO6, MJO9), braid-bar-mid (MJO4, MJO8) and braid-bar-tail (MJO3, MJO7) deposits were sampled to provide a comparative sample set to the material sampled from Fåbergstølsgrandane; K-feldspar luminescence signals were measured.

4.4. Sample collection

Samples from Nigardsdalen were collected in opaque plastic tubes using conventional OSL methods, whereby the tubes were hammered into a cleaned face of the sediment. Samples from Stordalen and Fåbergstølsgrandane were collected through covering the sample site with an opaque, plastic bag and clearing a face of at least 20 mm from the sediment to remove any bleached surface material prior to sampling. Light penetration has been shown not to affect D_e values after ~7 mm (Ollerhead, 2001). Samples were placed directly into transparent plastic bags within a second opaque bag, ensuring no light exposure occurred.

5. Methods

5.1. Sample preparation

Samples were prepared for OSL using conventional methods. Material was desiccated at 50 °C to enable calculation of water content, and sieved to extract the 180–212 μm grain size fraction. Approximately 10 g of the selected grain size fraction, dependent on sediment availability, was treated with 30% HCl for 30 min to remove $CaCO_3$ and then with H_2O_2 to remove organics. Density separations were used to extract the 2.58–2.68 gcm^{-3} quartz and <2.58 g cm^{-3} K-feldspar fractions. The quartz extract was etched with 40% HF for 40 min, to remove contaminating feldspars and the outer layer of the grains which has been affected by alpha irradiation. Etched quartz was treated with 30% HCl for 30 min to remove fluorides produced during etching. K-feldspar samples were not etched (Duller, 1992).

5.2. Luminescence measurements

All OSL analyses were carried out using either a TL-DA-15 (Bøtter-Jensen et al., 2003) or TL-DA-20 Risø reader, equipped with an EMI 9235QA photomultiplier. Quartz luminescence signals were detected in the UV through a 7.5 mm Hoya U-340 filter following blue stimulation (470 ± 20 nm), whereas K-feldspar luminescence signals were detected in the blue through a Corning 7-59 and BG-39 filter following IR stimulation (~870 nm). Irradiation was achieved using a $^{90}Sr/^{90}Y$ beta source with dose rates of 0.1 or 0.01 Gy s^{-1} dependent on instrument. Both readers were calibrated using quartz prepared at the Risø National Laboratory in Denmark. Measurements were plotted using Analyst v.3.22b (Duller, 2005). Quartz and K-feldspar were deposited in mono-layer onto stainless steel discs (9.8 mm Ø) using silicon grease and aliquot size was regulated using a large (7 mm Ø, ~400 grain) mask for quartz analyses and a small (2 mm Ø, ~30 grain) mask for K-feldspar analyses.

5.2.1. Quartz OSL

Both the quartz and K-feldspar samples were analysed using a single aliquot regenerative dose (SAR) protocol (Murray and Wintle, 2000, Table 1a) which involves interpolation of the natural luminescence signal (L_n) onto a dose response curve comprising the luminescence response (L_x) to multiple regenerative doses of different amounts (Fig. 7). All L_n and L_x measurements are interspaced by measurement of the luminescence response (T_x) to a test dose (T_D) of fixed amount, which is used to normalise the different measurements i.e. L_x/T_x. The protocol for the quartz samples was

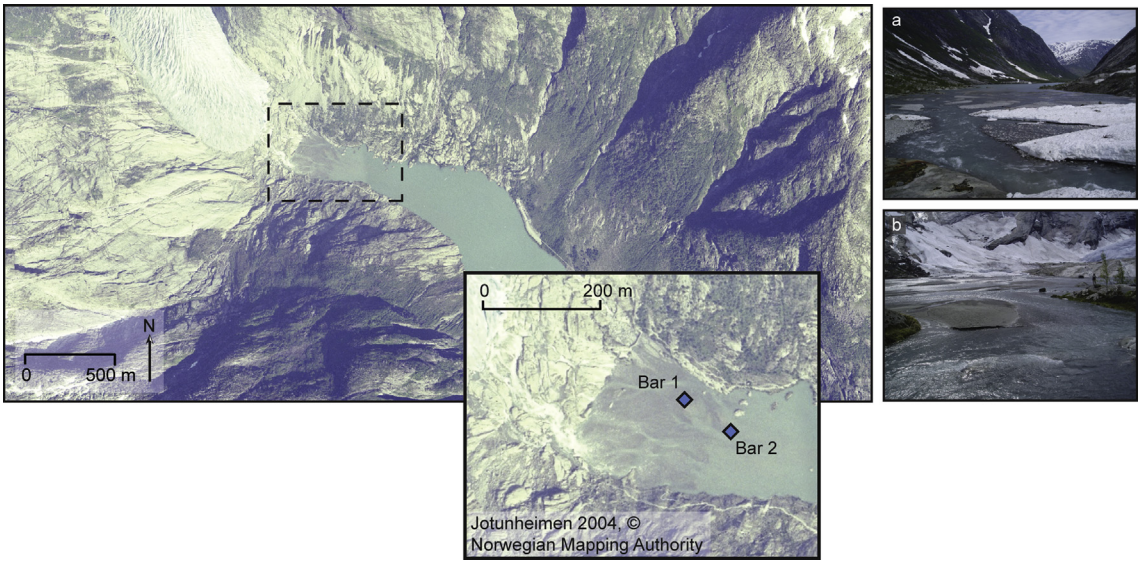

Fig. 6. Aerial photograph of Nigardsdalen showing the sampling locations of bars 1 and 2. a) Photograph looking across the Nigardsdalen proglacial data from the glacial snout and b) photograph looking across the proglacial delta towards to the glacial snout.

selected through testing a range of preheat temperatures and confirming that samples are able to recover a known laboratory dose.

Quartz analysed from Jostedalen has low luminescence sensitivity (Fig. 7a) which makes OSL analyses challenging, consequently it was necessary to relax the sample acceptance criteria thresholds relative to some other studies (e.g. Thrasher et al., 2009b). Sample acceptance criteria are that 1) recycling ratios (Murray and Wintle, 2000) are within 20% of unity, 2) signal intensities are $\geq 3\sigma$ above background, 3) recuperation is within 20% of the normalised maximum regenerated signal, and 4) IR depletion is within 20% of unity (Duller, 2003). Quartz optical stimulations were 40 s in duration; signals were integrated over the first 1.6 s and backgrounds over the final 8 s of stimulation. Quartz aliquot acceptance is 72% across all samples, with poor recycling and low signal intensities accounting for the rejection of ~18% of aliquots (see Supplementary Table S.1).

5.2.2. K-feldspar OSL

In contrast to the quartz samples, the K-feldspar samples had very bright luminescence sensitivity (Fig. 7b) and were measured using a modified SAR protocol (Table 1b), as proposed by Wallinga et al. (2007) whereby the first and second preheat temperatures are identical in order to improve sensitivity corrections (after Blair et al., 2005; Huot and Lamothe, 2003). A high-temperature IR bleach was also incorporated at the end of each SAR cycle (Murray and Wintle, 2003; Blair et al., 2005; Buylaert et al., 2007) which is designed to deplete excess signal that may accumulate throughout analysis (Table 1b). The suitability of the selected protocol was confirmed through a dose-recovery preheat-plateau experiment; doses were recovered within 10% of unity. The recently developed post-IR IRSL protocol (Thomsen et al., 2008; Buylaert et al., 2009) which is less susceptible to anomalous fading and is thought to provide more precise age determinations for K-feldspars (Buylaert et al., 2012) was only used to explore three samples as it is not suitable for young sediments or those that may be partially bleached (Thiel, 2011). A preheat of 250°C for 60 s was used, followed by an IR stimulation at 50°C for 100 s and a post-IR IR stimulation at 250°C for 100 s in a protocol modified from Buylaert et al. (2009). Both L_x and T_x measurement conditions were kept the same and a high temperature IR bleach at 290°C for 100 s was also incorporated at the end of each measurement cycle.

Acceptance criteria for the K-feldspar aliquots are that 1) recycling ratios are within 10% of unity; 2) signal intensities are $\geq 3\sigma$ above background; 3) recuperation is within 10% of the normalised maximum regenerated dose and 4) D_e value uncertainties are $\leq$10%. K-feldspar optical stimulations were 100 s in duration; signals were integrated over the first 4 s of stimulation, and background signals from the final 20 s of stimulation. K-feldspar aliquot acceptance is 98% across all samples; D_e values have not been corrected for anomalous fading, as differences in relative residual ages rather than the absolute residual ages, are of key interest.

Table 1a
Quartz SAR protocol.

Natural/Regenerative dose	5, 10, 20, 30, 0, 5, 5 Gy[a]
TL	180 °C, 10 s, 5 °C/s
IRSL	20 °C, 40 s, 5 °C/s (final cycle only)
OSL (L_n, L_x)	125 °C, 40 s, 5 °C/s
Test Dose (T_D)	5 Gy
TL	180 °C, 10 s, 5 °C/s
OSL (T_x)	125 °C, 40 s, 5 °C/s

[a] Regenerative doses varied dependent upon sample D_e values but initial analyses were carried out with these doses.

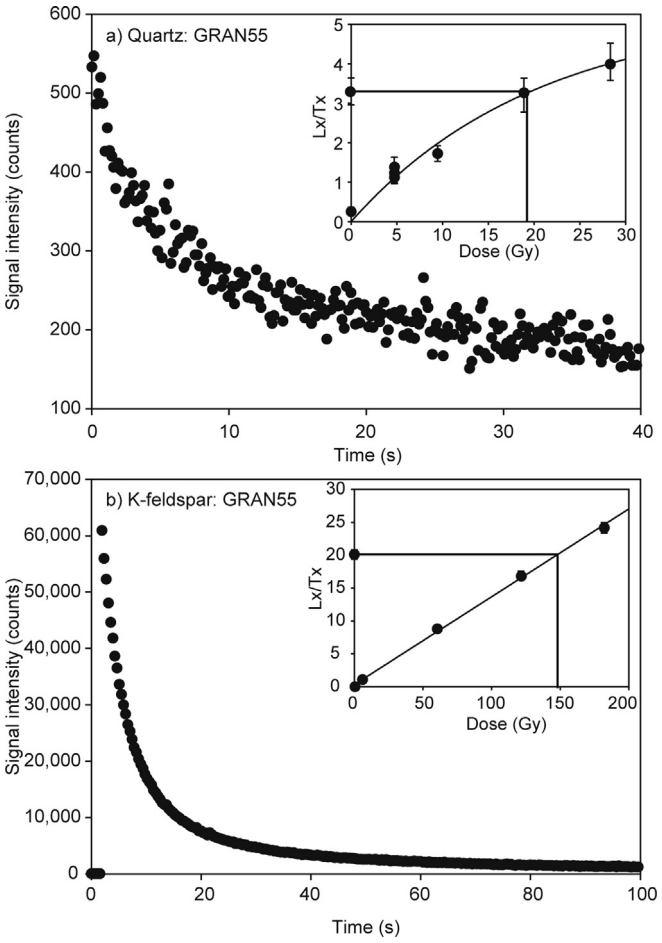

Fig. 7. Luminescence decay curve for an aliquot of a) the quartz and b) the K-feldspar extracts of sample GRAN55. Insets show the luminescence dose response curves for the same aliquots.

5.2.3. K-feldspar standardised growth curve

Standardised growth curves (SGCs) for quartz and polymineral fine grains have recently been investigated by a number of authors (e.g. Roberts and Duller, 2004; Burbidge et al., 2006; Telfer et al., 2008). A set of individual sample specific SGCs for samples which interpolate on the linear part of the dose response curve were developed for the K-feldspar samples as they behave in a uniform manner.

The sample specific SGCs were constructed from between twelve and twenty-four aliquots, which were measured using a full SAR protocol. Average dose response values (L_x/T_x) for different regenerative doses were normalised for T_D (Roberts and Duller, 2004) and fitted with a linear function to form SGCs from which D_e values could be interpolated. Inadequate data were available to generate SGCs beyond the linear part of the dose response curve, and two aliquots of sample LOD4 have been rejected as they interpolate beyond this range. The SGCs were tested through separating the SAR measured aliquots into two equal-sized populations, and constructing two different SGCs: one for each population (SGC_{P1} and SGC_{P2}). The SGC_{P1} was used to calculate SGC D_e values for aliquot population two, and vice versa (Table S.2); these SGC D_e values were then tested against the D_e values measured for the same aliquots within a full SAR protocol. All SGC/SAR D_e values were within 10% of unity.

Luminescence analyses for SGC interpolation comprised measurement of L_n/T_n followed by a single regenerative dose cycle

Table 1b
Feldspar SAR protocol.

Natural/Regenerative doses	6.2, 12.4, 18.6, 0, 6.2 Gy[a]
TL	250 °C, 60 s, 5 °C/s
IRSL (L_n, L_x)	50 °C, 100 s, 5 °C/s
Test Dose (T_D)	6.2 Gy
TL	250 °C, 60 s, 5 °C/s
IRSL (T_x)	50 °C, 100 s, 5 °C/s
IRSL	290 °C, 100 s, 5 °C/s

[a] Regenerative doses varied dependent upon sample D_e values but initial analyses were carried out with these doses.

(after Burbidge et al., 2006), where the regenerative dose was equal to the T_D. A T_D of 6.2 Gy was used throughout all analyses for SGC interpolation, which is equal to the T_D used in the K-feldspar SAR protocol for all samples. The two SGCs were combined to form a single sample specific SGC, which was used to calculate D_e values for that specific sample. Curve fit error was calculated using LINEST in Excel 2007, and incorporated together with 1.5% analytical error in D_e error estimations. Samples measured using an SGC are indicated in Table 2; SGC development greatly increased the rate of analysis.

5.2.4. Luminescence sample reproducibility

The highly overdispersed nature of the Norwegian sample suite (Fig. 1, Table 2) necessitates that sample reproducibility is investigated. This has been achieved through splitting one sandur side-attached bar sample (GRAN69) into two sub-samples (#1and #2) from which the K-feldspar extract was prepared and analysed separately. The overdispersion and D_e values of the K-feldspar sub-samples overlap within uncertainties, indicating that the luminescence behaviour is reproducible: overdispersion values are 64 ± 5% (GRAN69#1, $n = 24$) and 59 ± 3% (GRAN69#2, $n = 36$) and central-age modelled (CAM, Galbraith et al., 1999) D_e values are 13.47 ± 1.78 and 12.42 ± 1.22 Gy. As GRAN69#1 and GRAN69#2 are indistinguishable at 1σ uncertainties, they are considered as a single sample from this point forward (GRAN69).

5.2.5. Luminescence age modelling

The majority of samples analysed here are heterogeneously bleached, and produce a range of D_e values that are not normally distributed. These distributions can be characterised through calculation of the sample overdispersion; however, in order to contrast the residual ages of the different deposits, it is necessary to use an age model (Galbraith et al., 1999). Age models were selected using the criteria of Bailey and Arnold (2006) with revised critical values (Arnold, 2006) after Thrasher et al. (2009b) and results are summarised in Table 2.

5.3. Environmental radiation dose rate determination

The environmental radiation dose rate (D_r) must be determined in order to calculate sample residual age. It comprises external contributions from cosmic radiation and from the decay of radio-isotopes in the sedimentary matrix, as well as internal contributions from the decay of radio-isotopes within the mineral under investigation itself. Etching quartz removes the majority of the grain affected by external alpha irradiation, and no internal alpha dose rate is incorporated. As the K-feldspar samples analysed are not etched, an external alpha contribution to their D_r has been included. Alpha and beta attenuation factors after Bell (1980), Mejdahl (1979) and Readhead (2002a, b) have been used and conversion factors after Adamiec and Aitken (1998). A concentration of 12% K has been assumed for the internal β-dose of K-feldspar samples (Huntley and Baril, 1997), and an a-value of 0.15 ± 0.05 (Balescu and Lamothe, 1992). A cosmic dose rate contribution of 0.221 ± 0.022 Gy ka^{-1} has been incorporated, which was calculated using the factors of Prescott and Hutton (1994).

The concentrations of U, Th, K and Rb were measured directly using ICP-MS however it was not possible to measure radio-isotope concentrations for all samples. Where this is the case, the radio-isotope values of all other samples for that catchment have been averaged and the associated standard deviation calculated; these values are used to provide an approximate residual age and those samples where average D_r has been used are clearly identified in Table 3.

All of the samples analysed in this research are surface deposits, consequently the infinite matrix assumption made within most depositional settings is invalidated (Aitken, 1985). As gamma rays have a range of ~30 cm and the samples have been taken from ~2 cm below the ground surface, the samples will not have been subject to a complete gamma dose. The gamma dose rate

Table 2a
Feldspar model selection results.

Sample	Type	Facies	n	Average D_e (Gy)	D_e CAM	σ_d	$2\sigma c_w$	Norm c_w	c crit ($1/2\sigma c_w$)	$2\sigma k_w$	Norm k_w	k_w crit ($0.6/2\sigma k_w$)	Selected model	Modelled D_e (Gy)
LOD4[b]	Side-attached	Sh	46	27.11 ± 1.00	23.23 ± 1.80	0.525 ± 0.040	0.72	3.98	1.38	1.44	9.85	0.42	MAM-3	11.87 ± 1.02
LOD5	Bar	Sr	24	52.37 ± 2.24	46.02 ± 4.92	0.523 ± 0.029	1.00	1.28	1.00	2.00	0.89	0.30	MAM-3	6.99 ± 1.15
LOD6[b]		Sr	48	24.15 ± 0.80	18.51 ± 1.97	0.735 ± 0.065	0.71	1.48	1.41	1.41	−0.59	0.42	MAM-3	5.78 ± 0.66
GRAN69#1		Sr	24	17.35 ± 0.97	13.47 ± 1.78	0.644 ± 0.048	1.00	2.57	1.00	2.00	5.05	0.30	MAM-3	6.08 ± 0.76
GRAN69#2		Sr	36	14.80 ± 0.64	12.42 ± 1.22	0.588 ± 0.031	0.82	2.46	1.22	1.63	2.17	0.37	MAM-3	5.55 ± 0.55
GRAN69		Sr	60	15.82 ± 0.78	12.82 ± 1.02	0.612 ± 0.044	0.63	4.10	1.58	1.26	9.03	0.47	MAM-3	5.73 ± 0.44
GRAN54	Sandur	Sh	48	147.97 ± 5.17	145.77 ± 4.39	0.201 ± 0.010	0.71	0.04	1.41	1.41	−0.98	0.42	CAM	145.77 ± 4.39
GRAN55	Braid-bar	Sh	48	102.09 ± 3.25	99.10 ± 5.15	0.253 ± 0.005	0.71	0.71	1.41	1.41	−0.29	0.42	CAM	99.10 ± 0.05
GRAN56		Sr	55	320.80 ± 14.60	16.13 ± 0.53	0.244 ± 0.012	0.66	1.63	1.51	1.32	0.31	0.45	MAM-3	12.68 ± 0.69
GRAN57[b]		Sr	54	10.37 ± 0.37	12.98 ± 0.62	0.348 ± 0.020	0.67	1.71	1.50	1.33	0.11	0.45	MAM-3	8.56 ± 0.57
GRAN58		Sr	24	124.44 ± 4.30	120.99 ± 5.92	0.237 ± 0.004	1.00	−0.003	1.00	2.00	0.45	0.30	CAM	120.90 ± 36.08
GRAN59		Sr	60	173.28 ± 7.80	162.38 ± 5.00	0.234 ± 0.011	0.63	1.03	1.58	1.26	−0.18	0.47	L5%	103.72 ± 12.20
MJO3[b]	Delta	Sh	47	7.55 ± 0.46	7.27 ± 0.36	0.335 ± 0.021	0.72	8.12	1.40	1.43	25.69	0.42	MAM-3	6.27 ± 0.92
MJO4	Braid-bar	Sh	33	188.16 ± 9.95	164.56 ± 15.55	0.540 ± 0.027	0.85	1.49	1.17	1.71	0.81	0.35	MAM-3	69.71 ± 8.87
MJO6[a]		Sh	23	61.76 ± 3.69	50.09 ± 6.36	0.607 ± 0.043	1.02	1.23	0.98	1.02	2.04	5.88	MAM-3	7.45 ± 178.18
MJO7[b]		Sh	48	5.44 ± 0.25	4.89 ± 0.22	0.306 ± 0.018	0.71	4.78	1.41	1.41	10.81	0.42	MAM-3	3.56 ± 0.21
MJO8		Sh	48	7.27 ± 0.33	6.52 ± 0.21	0.224 ± 0.011	0.71	1.10	1.41	1.41	−0.06	0.42	L5%	4.62 ± 0.29
MJO9[a b]		Sr	48	17.36 ± 0.79	12.35 ± 1.34	0.751 ± 0.067	0.71	5.20	1.41	1.41	16.86	0.42	MAM-3	6.23 ± 17.56

[a] The MAM-3 returns very large uncertainties for these samples, therefore they have been modelled with the L5% model instead: MJO6 D_e = 14.29 ± 0.70 and MJO9 D_e = 3.84 ± 0.25 Gy
[b] Analysed with an SGC.

Table 2b
Quartz model selection results.

Sample	Type	Facies	n	Average D_e (Gy)	D_e CAM	σ_d	$2\sigma c_w$	Normc$_w$	c crit ($1/2\sigma c_w$)	$2\sigma k_w$	Norm k_w	k_w crit ($0.6/2\sigma k_w$)	Selected model	Modelled D_e (Gy)
GRAN54	Sandur	Sh	13	17.90 ± 3.74	17.91 ± 1.28	0	1.36	0.14	0.74	2.72	−1.09	0.22	CAM	17.91 ± 1.28
GRAN55	Braid-bar	Sh	32	10.86 ± 4.94	10.77 ± 0.78	0.27 ± 0.01	0.87	2.72	1.15	1.73	0.15	0.35	MAM-3	10.81 ± 3.17
GRAN56		Sr	25	1.87 ± 2.46	–[a]	0	1.07	1.54	0.94	2.14	−0.26	0.28	CAM[a]	1.65 ± 0.23
GRAN57		Sr	32	2.21 ± 1.70	–[a]	0	0.91	7.33	1.10	1.82	3.81	0.33	CAM[a]	3.08 ± 0.23
GRAN58		Sr	20	10.50 ± 4.09	11.50 ± 1.24	0.24 ± 0.01	1.10	1.92	0.91	2.19	0.42	0.27	MAM-3	11.72 ± 3.47
GRAN59		Sr	24	17.71 ± 5.52	16.94 ± 1.00	0.16 ± 0.00	1.00	1.91	1.00	2.00	−1.56	0.30	MAM-3	14.24 ± 2.06

[a] CAM calculated following the removal of negative values, following the Bailey and Arnold (2006) decision tree.

component of the total D_r has been adjusted to account for this using the factors presented in Table H.1 of Aitken (1985), assuming a sample depth below the surface of 3 cm (i.e. the mid-point of the sample) and a soil density of 2 g cm^{-3} ("Adjusted Gamma Dose Rate", Table 3). Following calculation of D_r (Gy ka^{-1}), sample age is calculated: Age (ka) = D_e/D_r.

6. Results

6.1. Stordalen: glaciofluvial side-attached bar deposits

The overdispersion values for the four side-attached bar deposits range from 53 ± 4% for LOD4 and 52 ± 3% for LOD5, to 74 ± 7% for LOD6 and 61 ± 4% for GRAN69. Overdispersion values increase with increasing transport distance from the sediment sources (Fig. 8a). Comparison of the three component minimum age (MAM-3, Galbraith and Laslett, 1993) modelled ages for these deposits shows that whereas LOD4 has the greatest residual age of 3.00 ± 0.38 ka, GRAN69 has the smallest residual age of 1.18 ± 0.13 ka, therefore overdispersion increases as residual age reduces (Fig. 8b).

6.2. Fåbergstølsgrandane: sandur braid-bar deposits

The overdispersion values for the sandur braid-bar deposits are low (<35%) for both the quartz and K-feldspar samples, relative to the side-attached bar deposits described from Stordalen and Fåbergstølsgrandane (Section 6.1, Table 2). Only minor modification of overdispersion with increasing sediment reworking across the bars is observed (Figs. 8a and 9), although braid-bar-tail deposits have greater overdispersion values than braid-bar-head deposits from the same bar feature (Table 4, Bar 1). Residual age reduces with increasing reworking across the composite bar forms (Fig. 9; Table 4). Samples GRAN54, GRAN58 and GRAN59 are sampled from braid-bar-head deposits and have the greatest residual ages (K-feldspar ages are ≥26.6 ka, quartz ages are ≥3.4 ka), GRAN55 is sampled from a braid-bar-mid and GRAN56 and GRAN57 are sampled from braid-bar-tails and have the lowest residual ages for both the K-feldspar and quartz fractions (K-feldspar ages are ≤2.8 ka, quartz ages are ≤0.9 ka). Bleaching six aliquots of the K-feldspar extract of sample GRAN56 for 300 min on a bright overcast day in July in St Andrews (Scotland, UK) resulted in measurement of a residual D_e value of 2.34 ± 0.12 Gy, suggesting that the bar-tail deposits measured from Fåbergstølsgrandane are completely bleached. Where the percentage reduction in age is considered between the braid-bar-head (GRAN54) and braid-bar-tail (GRAN56) deposits of a single bar feature (Bar 1), a reduction of 80–90% is observed in both the K-feldspar and quartz OSL residual ages (Table 4).

In addition to measuring the IRSL$_{50}$ signal a post-IR IRSL$_{250}$ measurement was also made following preheating at 250°C on twelve aliquots of braid-bar-head deposit GRAN54, bar-mid deposit GRAN55 and bar-tail deposit GRAN56. The CAM D_e values of these measurements are 482 ± 27 Gy (σ_d = 18 ± 2%), 316 ± 15 Gy (σ_d = 16 ± 1%) and 91 ± 3 Gy (σ_d = 12 ± 1%) respectively, and also exhibit a signal reduction of 80%. These unbleached residual values are much greater than the post-IR IRSL$_{290}$ residuals of 27–31 Gy reported by Alexanderson and Murray (2012a) for their modern sandur deposits, and is anticipated because post-IR IRSL signals are less readily bleached (cf. Murray et al., 2012). However it should also be noted that use of a 250°C preheat temperature, rather than a temperature greater than the post-IR IRSL stimulation temperature, may also have exacerbated these residuals. These data are presented as they will be of interest to researchers who wish to utilise post-IR IRSL dating methods in glacial settings.

6.3. Nigardsdalen: proglacial delta braid-bar deposits

The luminescence properties of the Nigardsdalen samples contrast with the luminescence properties of samples from Fåbergstølsgrandane; the residual ages in Nigardsdalen are much lower and the overdispersion values are much greater and reduce with transport across braid-bar features (Figs. 8a and 10, Table 5). The residual ages of the Nigardsdalen samples, calculated with the lowest 5% (L5%, Olley et al., 1998) and MAM3 models are lower for Bar 2 than Bar 1 (Table 5). No uniform reduction in residual age across Bar 2 is observed and braid-bar-mid sample MJO4 (Bar 1) has a much greater residual age (19.00 ± 3.02 ka) than the other Nigardsdalen samples. The braid-bar-head deposits (MJO6 and MJO9) in Nigardsdalen have residual ages of 3.18 ± 0.31 and 0.96 ± 0.11 ka, ≥23 ka lower than equivalent deposits in Fåbergstølsgrandane, and overdispersion values are 61 ± 4% and 75 ± 7% which are twice as large as the equivalent Fåbergstølsgrandane deposits (Tables 4 and 5).

7. Discussion

7.1. Valley main meltwater channel side-attached bar deposits

The four side-attached bar deposits analysed (LOD4, LOD5, LOD6 and GRAN69) have similar source sediments and exhibit reducing residual ages and increasing overdispersion values as transport distances increase (Fig. 8a). This can be explained by improved sediment bleaching with increasing transport distance in the Stordalen and Fåbergstølsgrandane main-meltwater channels, and is in agreement with observations by other luminescence practitioners working in glacial and fluvial environments (e.g. Forman and Ennis, 1992; Stokes et al., 2001).

The residual ages of the side-attached bar deposits range from 3.00 ± 0.38 ka for LOD4 which is the most ice-proximal sample (1.3 km distant), to 1.18 ± 0.13 ka for GRAN69 which is the sample furthest from the ice-front (6.7 km distant). The unbleached residual ages presented here suggest that the IRSL$_{50}$ signal of side-attached bar deposits will retain residual ages of 1.5–3 ka (~6–

Table 3a
Dosimetry and age calculations for the feldspar samples analysed. Beta-particle attenuation factors of 0.80 (^{40}K), 0.89 (^{232}Th), 0.93 (^{238}U) and 0.34 (^{87}Rb) have been used after Mejdahl (1979) and Readhead (2002a, b) respectively. Cosmic dose rates have been calculated using the method of Prescott and Hutton (1994), assuming an overburden density of 2 g cm^{-3} and sample depth of 2 cm.

Sample	Type	n	D_e (Gy)	Age model	Water content (%)	K (%)	Th (ppm)	U (ppm)	Rb (ppm)	Dry alpha dose rate (Gy ka^{-1})	Dry gamma dose rate (Gy ka^{-1})	Adjusted gamma dose rate (Gy ka^{-1})	Water Attenuated dose rate (Gy ka^{-1})	Age (ka)
LOD4[a,b,c]	Side-attached bar	46	11.87 ± 1.02	MAM-3	15	2.89 ± 0.14	13.53 ± 1.87	2.91 ± 0.73	121.8 ± 4.5	0.34 ± 0.35	1.19 ± 0.09	0.95 ± 0.10	3.96 ± 0.36	3.00 ± 0.38
LOD5[a]		24	6.99 ± 1.15	MAM-3	21	2.89 ± 0.14	13.53 ± 1.87	2.91 ± 0.73	121.8 ± 4.5	0.34 ± 0.35	1.19 ± 0.09	0.95 ± 0.10	3.77 ± 0.34	1.89 ± 0.35
LOD6[a,b]		48	5.78 ± 0.66	MAM-3	19	2.89 ± 0.14	13.53 ± 1.87	2.91 ± 0.73	121.8 ± 4.5	0.34 ± 0.35	1.19 ± 0.09	0.95 ± 0.10	3.82 ± 0.34	1.51 ± 0.22
GRAN69a		24	6.08 ± 0.76	MAM-3	14	2.89 ± 0.14	14.85 ± 0.74	3.42 ± 0.17	118.6 ± 4.5	0.38 ± 0.36	1.80 ± 0.07	1.27 ± 0.05	4.84 ± 0.37	1.26 ± 0.19
GRAN69b		36	5.55 ± 0.55	MAM-3	14	2.89 ± 0.14	14.85 ± 0.74	3.42 ± 0.17	118.6 ± 4.5	0.38 ± 0.36	1.80 ± 0.07	1.27 ± 0.05	4.84 ± 0.37	1.15 ± 0.15
GRAN69		60	5.73 ± 0.44	MAM-3	14	2.89 ± 0.14	14.85 ± 0.74	3.42 ± 0.17	118.6 ± 4.5	0.38 ± 0.36	1.80 ± 0.07	1.27 ± 0.05	4.84 ± 0.37	1.18 ± 0.13
GRAN54[a]	Sandur Braid-bar	48	145.77 ± 4.39	CAM	22	2.89 ± 0.14	13.53 ± 1.87	2.91 ± 0.73	121.8 ± 4.5	0.34 ± 0.45	1.19 ± 0.09	0.95 ± 0.10	4.33 ± 0.41	33.64 ± 3.49
GRAN55[a]		48	99.10 ± 5.15	CAM	23	2.89 ± 0.14	13.53 ± 1.87	2.91 ± 0.73	121.8 ± 4.5	0.34 ± 0.45	1.19 ± 0.09	0.95 ± 0.10	4.35 ± 0.41	22.79 ± 2.53
GRAN56a[b]		55	12.68 ± 0.69	MAM-3	16	2.89 ± 0.14	13.53 ± 1.87	2.91 ± 0.73	121.8 ± 4.5	0.34 ± 0.45	1.19 ± 0.09	0.95 ± 0.10	4.59 ± 0.44	2.77 ± 0.32
GRAN57a[b]		54	8.56 ± 0.57	MAM-3	24	2.89 ± 0.14	13.53 ± 1.87	2.91 ± 0.73	121.8 ± 4.5	0.34 ± 0.45	1.19 ± 0.09	0.95 ± 0.10	4.32 ± 0.41	1.98 ± 0.24
GRAN58[a]		24	120.90 ± 36.07	CAM	17	2.89 ± 0.14	13.53 ± 1.87	2.91 ± 0.73	121.8 ± 4.5	0.34 ± 0.45	1.19 ± 0.09	0.95 ± 0.10	4.55 ± 0.43	26.59 ± 8.36
GRAN59[a]		60	103.72 ± 12.20	L5%	11	2.89 ± 0.14	13.53 ± 1.87	2.91 ± 0.73	121.8 ± 4.5	0.34 ± 0.45	1.19 ± 0.09	0.95 ± 0.10	4.79 ± 0.47	26.87 ± 3.08
MJO3[a,b]	Delta Braid-bar	47	6.27 ± 0.92	MAM-3	24	3.17 ± 0.16	12.93 ± 0.75	2.21 ± 0.13	131.80 ± 6.59	0.30 ± 0.35	1.64 ± 0.07	1.16 ± 0.05	3.69 ± 0.33	1.45 ± 0.24
MJO4		33	69.71 ± 8.87	MAM-3	22	3.38 ± 0.17	10.96 ± 0.64	1.60 ± 0.09	135.60 ± 6.78	0.24 ± 0.34	1.52 ± 0.07	1.08 ± 0.05	3.67 ± 0.33	19.00 ± 3.02
MJO6		23	14.29 ± 0.70	L5%	22	3.46 ± 0.17	12.43 ± 0.73	1.76 ± 0.10	141.30 ± 7.07	0.27 ± 0.35	1.64 ± 0.07	1.16 ± 0.05	3.84 ± 0.34	3.18 ± 0.31
MJO7[b]		48	3.56 ± 0.21	MAM-3	15	3.06 ± 0.15	12.37 ± 0.72	2.31 ± 0.12	125.60 ± 6.28	0.29 ± 0.35	1.59 ± 0.07	1.13 ± 0.05	3.90 ± 0.35	0.91 ± 0.10
MJO8[b]		48	4.62 ± 0.29	L5%	21	3.09 ± 0.15	12.15 ± 0.71	2.34 ± 0.14	131.60 ± 6.58	0.29 ± 0.35	1.59 ± 0.07	1.13 ± 0.05	3.73 ± 0.34	1.24 ± 0.14
MJO9[b]		48	3.84 ± 0.25	L5%	19	2.88 ± 0.14	16.65 ± 0.97	3.07 ± 0.18	124.90 ± 6.25	0.39 ± 0.36	1.84 ± 0.07	1.30 ± 0.05	3.55 ± 0.20	0.96 ± 0.11

[a] Average dose rate used to calculate age.
[b] Analysed with an SGC.
[c] Two aliquots of LOD4 were rejected as the D_e interpolates beyond the SGC.

12 Gy) when sampled within 2 km of the ice-front, which would result in age overestimations if Holocene or Last Glacial Maximum sediments are dated. Few recent studies have reported residual luminescence signals for the $IRSL_{50}$ signal of K-feldspar from fluvial or glaciofluvial sediments although Alexanderson and Murray (2012a) report $IRSL_{50}$ residual signals of ~12 Gy for ice-proximal deposits from Svalbard, which are similar to the ~6–12 Gy residual signals reported for the side-attached bar deposits measured here. These ages are older than quartz unbleached residual ages reported for glacial and fluvial sediments in some studies (e.g. Jaiswal et al., 2009; Alexanderson and Murray, 2012a, 2012b) but are comparable to others (e.g. Hu et al., 2010) and are similar to quartz residuals from neighbouring catchment Fåbergstølsdalen (King et al., 2013). Therefore these results are promising, as they show that in some glacial settings the $IRSL_{50}$ signal of K-feldspar is bleached to a similar extent as the quartz signal, despite the various empirical observations which have shown that K-feldspars bleach less rapidly (e.g. Klasen et al., 2006).

7.2. Braid-bar deposits

7.2.1. Fåbergstølsgrandane

In contrast to the glaciofluvial side-attached bar deposits analysed from Stordalen, the Fåbergstølsgrandane sandur is relatively distant from the ice margins of Lodalsbreen and Stigaholtsbreen (~6 km). Consequently it is surprising that the braid-bar-head residual ages are so large (K-feldspar $IRSL_{50}$ ages are ≥26.6 ka (≥103 Gy), quartz ages are ≥3.4 ka (≥11.7 Gy)) as glaciofluvial sediments have been shown to bleach effectively within this glaciofluvial environment over relatively short transport distances (i.e. the residual ages of the Stordalen side-attached bar deposits discussed in Section 7.1). These unbleached residual ages are also much greater than those reported for a modern sandur bar (3 km from the glacier margin, specific position on the bar unspecified) and river bank deposit by Alexanderson and Murray (2012a), for which they recorded $IRSL_{50}$ unbleached residual signals of 3.2–5.2 Gy. The high unbleached residual ages reported here are a consequence of the specific transport and depositional process that the sediments have experienced, and can be explained by the specific location of the braid-bar deposits sampled from Fåbergstølsgrandane. The braid-bars sampled are ~200 m from the main meltwater channel, and consequently will only be activated during periods of peak discharge following episodic storm or snowmelt events. Such events result in high energy pulses of material onto the sandur, and will offer limited opportunity for bleaching due to high suspended sediment loads and turbulent flow (e.g. Ditlefsen, 1992). Braid-bar-head deposits essentially comprise channel material, which is known to sort less rapidly than material transported across channel bars (Rice and Church, 2010) and thus poorly sorted sediments are likely to be less effectively bleached than well sorted sediments. The sensitivity of the OSL signal to such differences in depositional processes demonstrates its use as an indicator of transport and depositional process.

The unbleached residuals measured for the braid-bar head deposits are greater than those reported for quartz measurements of subglacial sediments from neighbouring Fåbergstølsdalen. King et al. (2013) reported residual ages of up to only 1.72 ± 0.77 ka, which were lower than anticipated for an *in-situ* deposit. They attributed the relatively low residuals to potential partial resetting of the sediments which were at the front of the glacier, or alternatively to the incorporation of reset grains from the glacier margins. Whereas their subglacial samples had high overdispersion values of ~70%, the Fåbergstølsgrandane braid-bar samples have relatively low overdispersion values (Table 4), suggesting that they have not been significantly heterogeneously bleached. The K-

Table 3b
Dosimetry and age calculations for the quartz samples analysed.

Sample	Type	n	D_e (Gy)	Model	Water content (%)	K (%)	Th (ppm)	U (ppm)	Rb (ppm)	Dry alpha dose rate (Gy ka^{-1})	Dry gamma dose rate (Gy ka^{-1})	Adjusted gamma dose rate (Gy ka^{-1})	Water Attenuated dose rate (Gy ka^{-1})	Age (ka)
GRAN54[a]	Sandur Braid-bar	13	17.91 ± 1.28	CAM	22	2.89 ± 0.17	13.53 ± 1.92	2.91 ± 0.73	121.8 ± 4.53	–	1.19 ± 0.09	0.95 ± 0.10	3.32 ± 0.22	5.39 ± 0.55
GRAN55[a]		32	10.81 ± 3.17	MAM-3	23	2.89 ± 0.17	13.53 ± 1.92	2.91 ± 0.73	121.8 ± 4.53	–	1.19 ± 0.09	0.95 ± 0.10	3.29 ± 0.21	3.29 ± 1.00
GRAN56[a]		25	1.65 ± 0.23	CAM	16	2.89 ± 0.17	13.53 ± 1.92	2.91 ± 0.73	121.8 ± 4.53	–	1.19 ± 0.09	0.95 ± 0.10	3.51 ± 0.23	0.47 ± 0.07
GRAN57[a]		32	3.08 ± 0.23	CAM	24	2.89 ± 0.17	13.53 ± 1.92	2.91 ± 0.73	121.8 ± 4.53	–	1.19 ± 0.09	0.95 ± 0.10	3.26 ± 0.21	0.94 ± 0.10
GRAN58[a]		20	11.72 ± 3.47	MAM-3	17	2.89 ± 0.17	13.53 ± 1.92	2.91 ± 0.73	121.8 ± 4.53	–	1.19 ± 0.09	0.95 ± 0.10	3.47 ± 0.23	3.38 ± 1.03
GRAN59[a]		24	14.24 ± 2.06	MAM-3	11	2.89 ± 0.17	13.53 ± 1.92	2.91 ± 0.73	121.8 ± 4.53	–	1.19 ± 0.09	0.95 ± 0.10	3.70 ± 0.24	3.85 ± 0.62

[a] Average dose rate used to calculate age.

feldspar overdispersion values range from 20 to 24% and quartz values range from 16 to 24%. Because the sample overdispersion values are mostly >20% it is likely that these sediments have been partially bleached during transport and deposition, rather than not bleached at all (Galbraith et al., 1999; Arnold and Roberts, 2009). Although their low overdispersion values are more characteristic of type 'A' sediments which have experienced near-homogeneous partial bleaching, rather than type 'B' sediments which have been bleached heterogeneously and so exhibit greater overdispersion values (Duller, 1994).

The measured luminescence signals of the K-feldspar extracts result in greater ages than their partner quartz extracts for all of the Fåbergstølsgrandane samples analysed in this study, which can be explained by slower bleaching of the K-feldspar luminescence signal relative to the quartz luminescence signal (e.g. Spooner, 1994; Wallinga, 2002; Klasen et al., 2006). In contrast, transport across braided channel bars enables improved sediment sorting and greater opportunities for bleaching of the luminescence signal for sediments deposited at the braid-bar-mids and −tails. During transport across the bar features, sediments are homogeneously, rather than heterogeneously bleached, as heterogeneous bleaching is anticipated to result in increasing overdispersion of the D_e value distributions as some grains became more fully reset (Table 4). It is interesting that the rate of signal depletion is equal for both the quartz and K-feldspar D_e values (Table 4), and shows that the luminescence signals of both minerals bleach at the same rate in some depositional settings (e.g. Sanderson et al., 2007).

7.2.2. Nigardsdalen

The high overdispersion values and low residual ages of the braid-bar-head deposits from Nigardsdalen shows that they have

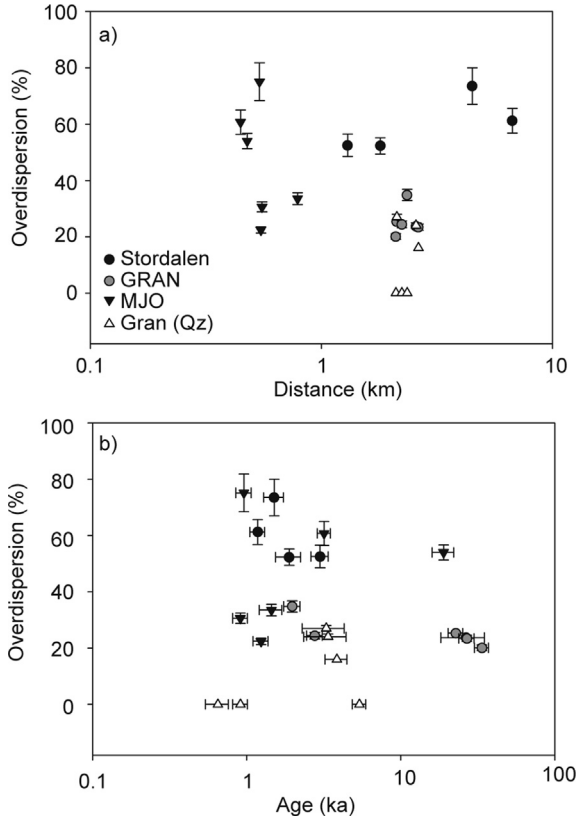

Fig. 8. Changing sample overdispersion values with a) transport distance and b) sample age.

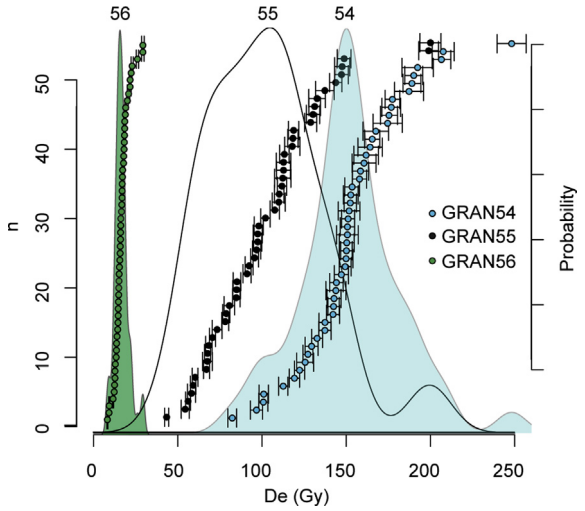

Fig. 9. D_e value distributions from 0 to 250 Gy for K-feldspar extracts of samples GRAN54 (braid-bar-head, $\sigma_d = 20 \pm 1\%$), GRAN55 (braid-bar-mid, $\sigma_d = 25 \pm 1\%$) and GRAN56 (braid-bar-tail, $\sigma_d = 24 \pm 1\%$) sampled from the same bar feature.

experienced greater sediment bleaching than the braid-bar-head deposits sampled from Fåbergstølsgrandane (Table 5), despite their relatively short transport distances (200–300 m). This can be explained by the greater opportunities for sediment bleaching within a channel of shallow relief, where sediments may be exposed multiple times during reworking across bar features.

The residual ages of the Nigardsdalen samples are lower for Bar 2 than Bar 1 (Table 5), which is attributed to greater bleaching opportunities with increasing transport distance, as has been recorded for the side attached-bar deposits sampled from Stordalen (Section 7.1). No uniform reduction in residual age across Bar 2 is observed, which may be a consequence of the almost fully bleached nature of these deposits (Table 5). Overdispersion and residual age reduce with reworking across the bar features (Fig. 8, Table 5) as sediment bleaching increases. If this bleaching is homogeneous and all grains bleach at the same rate, it may be anticipated that overdispersion values of the braid-bar-head deposits would be preserved (e.g. Fig. 9), however this is not recorded (Fig. 10). Homogeneous bleaching can cause a reduction in overdispersion where sediments are becoming fully bleached, and the smallest unbleached residual D_e values measured for MJO7 are ~3 Gy, which are similar to the D_e value of 2.34 ± 0.12 Gy measured for 6 aliquots of GRAN56 following 300 min of bleaching in sunlight. Therefore at least some grains of samples MJO3, MJO7, MJO8 and MJO9 are fully bleached. It can also be inferred that the same processes of sediment bleaching are occurring on both the sandur braid-bar deposits from Fåbergstølsgrandane, and the proglacial delta braid-bar deposits from Nigardsdalen.

Braid-bar-mid sample MJO4 has a much greater residual age (19.00 ± 3.02 ka) than the other Nigardsdalen samples, which is related to its specific sample location, adjacent to a crossover chute channel on Bar 1 (Fig. 3). Its relatively high age can be explained by the deposition of sediments transported via crossover flow during periods of elevated discharge when sediments are reworked across the proglacial delta more rapidly, resulting in reduced bleaching opportunities and illustrating the control that specific depositional setting has on sediment OSL properties.

7.3. Synthesis. This study has investigated the luminescence properties of glaciofluvial sediments from three different catchments. Residual ages and overdispersion values are sensitive to the specific depositional processes. Despite having similar source sediments, whereas side-attached bar deposits from Stordalen and Fåbergstølsgrandane and braid-bar-head deposits from Nigardsdalen have low residual ages but high overdispersion values, braid-bar-head deposits from Fåbergstølsgrandane have high residual ages and low overdispersion values. In Fåbergstølsgrandane, the high residual ages and low overdispersion values of the braid-bar-head deposits reflect the limited bleaching opportunities of source sediments with high residual ages transported onto the sandur during storm events and periods of peak snowmelt. In contrast, the low residual ages and high overdispersion values of the Nigardsdalen braid-bar-head deposits are a consequence of multiple bleaching opportunities within a catchment with low relief. Sediment sources and processes of transport across the braid-bar features are similar in both catchments, although the frequency of transport events is likely to be higher in Nigardsdalen because it is a relatively low relief system. Homogeneous bleaching of the Fåbergstølsgrandane sediments results in little variation in overdispersion values as a function of transport distance (Figs. 8 and 9); in contrast, the braid-bar deposits in Nigardsdalen exhibit a marked reduction in overdispersion values as sediments become completely bleached during reworking across bar-features (Figs. 8 and 10).

8. Conclusions and implications for successful sampling strategies

The Fåbergstølsgrandane sandur braid-bar deposits have greater residual ages than the proglacial delta braid-bar and main valley or sandur meltwater channel side-attached bar deposits. They exhibit the greatest residuals at the braid-bar-heads which are caused by initial deposition of poorly sorted sediments that have been poorly bleached during highly competent flow. Using overdispersion values alone it is not possible to discriminate between sediments

Table 4
Summary of Fåbergstølsgrandane sandur braided bar data.

		Bar head (a)	Bar mid	Bar tail (b)	% Change a → b	Bar head (a)	Bar mid	Bar tail (b)	% Change a → b
Bar 1		GRAN54	GRAN55	GRAN56		GRAN54Q	GRAN55Q	GRAN56Q	
	ka	33.64 ± 3.49	22.79 ± 2.53	2.77 ± 0.32	91.77%	5.39 ± 0.55	3.29 ± 0.21	0.47 ± 0.07	91.28%
	σ_d	20 ± 1	25 ± 1	24 ± 1		0	27 ± 1	0	
Relative transport distance (m)		*0* →	*53* →	*163*		*0* →	*53* →	*163*	
Bar 2a[a]		GRAN58		GRAN57		GRAN58Q		GRAN57Q	
	ka	26.59 ± 8.36	–	1.98 ± 0.24	92.55%	3.38 ± 1.03	–	0.94 ± 0.10	72.19%
	σ_d	0.24 ± 0.00	–	0.35 ± 0.02		0.24 ± 0.01	–	0	
Bar 2b[a]		GRAN59		GRAN57		GRAN59Q		GRAN57Q	
	ka	26.87 ± 3.08	–	1.98 ± 0.24	92.63%	3.85 ± 0.62	–	0.94 ± 0.10	75.58%
	σ_d	0.23 ± 0.01	–	0.35 ± 0.02		0.16 ± 0.00	–	0	
Average Signal Change:					92.32 ± 0.48%				79.68 ± 10.19%

[a] Composite bar forms: the bar-head and bar-tail deposits are taken from different bar features but are contrasted to explore changing residual age values.

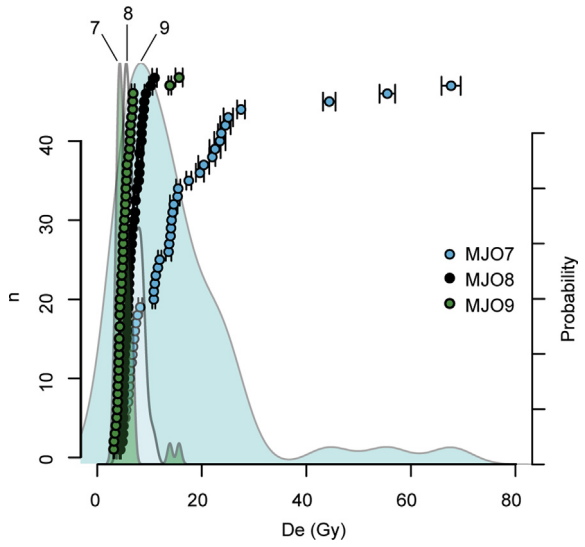

Fig. 10. D_e value distributions from 0 to 80 Gy for K-feldspar extracts of samples MJO9 (braid-bar-head, $\sigma_d = 61 \pm 4\%$), MJO8 (braid-bar-mid, $\sigma_d = 54 \pm 3\%$) and MJO7 (braid-bar-tail, $\sigma_d = 34 \pm 2\%$) sampled from the same bar-feature.

which remain almost completely unbleached, and sediments which have been well bleached prior to deposition. Consequently braid-bar-head deposits should not be sampled for OSL dating, and sample selection must be based on specific depositional setting and deposit sedimentology (c.f. Fuchs and Owen, 2008). Braid-bar-tail deposits have the smallest residual ages, which is in agreement with the findings of previous research (e.g. Thrasher et al., 2009b). The $IRSL_{50}$ K-feldspar signal is almost completely bleached for the proglacial delta braid-bar-tail deposits measured. Quartz and K-feldspar have been shown to bleach at the same rate during transport across bar features in Fåbergstølsgrandane, suggesting that although a residual of ~2 ka remains, the $IRSL_{50}$ signal of K-feldspar may also be appropriate for dating sandur braid-bar-tails, circumventing the challenges of dimly luminescent quartz (e.g. Rhodes and Bailey, 1997). These results may improve both sampling and luminescence analysis protocols for glacial sediments which can be challenging to date using luminescence methods.

The contrasting residual ages and overdispersion values identified between the similar depositional environments of Nigardsdalen and Fåbergstølsgrandane highlights the sensitivity of the luminescence signal to both the processes of sedimentation and specific depositional settings. In order to accurately quantify the luminescence properties of modern analogue deposits, it is essential that the deposit sedimentology and specific depositional setting of the samples are carefully characterised so that an appropriate modern analogue deposit is selected. It is preferable that multiple modern analogue samples are taken to avoid biasing results by localised effects e.g. at MJO4 high residual ages are the consequence of a crossover channel on the bar feature, and are not representative of the braid-bar-head or braid-bar-tail characteristics.

Table 5
Summary of Nigardsdalen delta braided bar data.

	Bar head (a)	Bar mid	Bar tail (b)	% Change a → b
Bar 1	MJO6	MJO4	MJO3	
ka	3.18 ± 0.31	19.00 ± 3.02	1.45 ± 0.24	54.40%
σ_d (%)	61 ± 4	54 ± 3	34 ± 2	
Relative transport distance (m)	*0* →	*45* →	*72*	
Bar 2	MJO9	MJO8	MJO7	
Ka	0.96 ± 0.11	1.24 ± 0.14	0.91 ± 0.10	5.21%
σ_d (%)	75 ± 7	22 ± 1	31 ± 2	
Relative transport distance (m)	*0* →	*28* →	*38*	
Average Signal Change:				29.81 ± 34.78%

Acknowledgements

GEK was supported by NERC studentship F008589/1 and was a SAGES affiliated student. R.Sommerville, A. Calder and D. Herd (University of St Andrews) and L. Carmichael and S.Fisk (SUERC) are thanked for laboratory assistance. D. Sanderson (SUERC) is thanked for useful discussions regarding the project, and for access to facilities at SUERC. D. Lowry (University of St Andrews), E. Harris (Swansea University), Liselotte, C. Caballero and A.Cullens (IceTroll) are thanked for fieldwork assistance. Financial support in the form of a New Workers Research Award is acknowledged from the QRA. Two anonymous reviewers are thanked for their comments which greatly improved an earlier version of this manuscript.

Appendix A. Supplementary data

Supplementary data related to this article can be found at http://dx.doi.org/10.1016/j.quascirev.2014.02.001.

References

Adamiec, G., Aitken, M.J., 1998. Dose-rate conversion factors: update. Anc. TL 16, 37–46.
Aitken, M.J., 1985. Thermoluminescence Dating. Academic Press, London.
Alexanderson, H., Murray, A.S., 2012a. Luminescence signals from modern sediments in a glaciated bay, NW Svalbard. Quat. Geochronol. 10, 250–256.
Alexanderson, H., Murray, A.S., 2012b. Problems and potential of OSL dating Weichselian and Holocene sediments in Sweden. Quat. Sci. Rev. 44, 37–50.
Arnold, L.J., 2006. Optical Dating and Computer Modelling of Arroyo Epicycles in the American Southwest. St Peter's College, University of Oxford.
Arnold, L.J., Bailey, R.M., Tucker, G.E., 2007. Statistical treatment of fluvial dose distributions from southern Colorado arroyo deposits. Quat. Geochronol. 2, 162–167.
Arnold, L.J., Roberts, R.G., 2009. Stochastic modelling of multi-grain equivalent dose (D_e) distributions: implications for OSL dating of sediment mixtures. Quat. Geochronol. 4, 204–230.
Bailey, R.M., Arnold, L.J., 2006. Statistical modelling of single grain quartz D-e distributions and an assessment of procedures for estimating burial dose. Quat. Sci. Rev. 25, 2475–2502.
Balescu, S., Lamothe, M., 1992. The blue emission of K-feldspar coarse grains and its potential for overcoming TL age underestimation. Quat. Sci. Rev. 11, 45–51.
Ballantyne, C.K., 1995. Paraglacial debris-cone formation on recently deglaciated terrain, western Norway. Holocene 5, 25–33.
Ballantyne, C.K., Benn, D.I., 1994. Paraglacial slope adjustment and resedimentation following recent glacier retreat, fåbergstølsdalen, Norway. Arct. Alp. Res. 26, 255–269.
Bateman, M.D., Boulter, C.H., Carr, A.S., Frederick, C.D., Peter, D., Wilder, M., 2007. Detecting post-depositional sediment disturbance in sandy deposits using optical luminescence. Quat. Geochronol. 2, 57–64.
Bell, W.T., 1980. Alpha dose attenuation in quartz grains for thermoluminescence dating. Anc. TL 12, 4–8.
Blair, M.W., Yukihara, E.G., McKeever, S.W.S., 2005. Experiences with single-aliquot OSL procedures using coarse-grain feldspars. Radiat. Meas. 39, 361–374.
Bøtter-Jensen, L., McKeever, S.W.S., Wintle, A.G., 2003. Optically Stimulated Luminescence Dosimetry. Elsevier Science, Amsterdam.
Boyce, J.I., Eyles, N., 2000. Architectural element analysis applied to glacial deposits: internal geometry of a late Pleistocen till sheet, Ontario, Canada. Bull. Geol. Soc. Am. 112, 98–118.
Bronk Ramsey, C., 2013. OxCal.
Brookfield, M.E., Martini, I.P., 1999. Facies architecture and sequence stratigraphy in glacially influenced basins: basic problems and water-level/glacier input-point controls (with an example from the Quaternary of Ontario, Canada). Sediment. Geol. 123, 183–197.
Bryhni, I., Sturt, B.A., 1985. Caledonides of southwestern Norway. In: Gee, D.E., Sturt, B.A. (Eds.), The Caledonide Orogen. John Wiley & Sons, Chichester, p. 619.
Burbidge, C.I., Duller, G.A.T., Roberts, H.M., 2006. D-e determination for young samples using the standardised OSL response of coarse-grain quartz. Radiat. Meas. 41, 278–288.

Buylaert, J.-P., Jain, M., Murray, A.S., Thomsen, K.J., Thiel, C., Sohbati, R., 2012. A robust feldspar luminescence dating method for Middle and Late Pleistocene sediments. Boreas 41, 435–451.
Buylaert, J.P., Murray, A.S., Thomsen, K.J., Jain, M., 2009. Testing the potential of an elevated temperature IRSL signal from K-feldspar. Radiat. Meas. 44, 560–565.
Buylaert, J.P., Vandenberghe, D., Murray, A.S., Huot, S., De Corte, F., Van den Haute, P., 2007. Luminescence dating of old (>70 ka) Chinese loess: a comparison of single-aliquot OSL and IRSL techniques. Quat. Geochronol. 2, 9–14.
Church, M., Ryder, J.M., 1972. Paraglacial sedimentation: a consideration of fluvial processes conditioned by glaciation. Geol. Soc. Am. Bull. 83, 3059–3071.
Curry, A.M., 1999. Paraglacial modification of slope form. Earth Surf. Process. Landf. 24, 1213–1228.
Curry, A.M., Ballantyne, C.K., 1999. Paraglacial modification of Glacigenic sediment. Geogr. Ann. Ser. A, Phys. Geogr. 81, 409–419.
Dahl, S.O., Nesje, A., Lie, Ø., Fjordheim, K., Matthews, J.A., 2002. Timing, equilibrium-line altitudes and climatic implications of two early-Holocene glacier readvances during the Erdalen Event at Jostedalsbreen, western Norway. Holocene 12, 17–25.
Ditlefsen, C., 1992. Bleaching of K-feldspars in turbid water suspensions: a comparison of photo- and thermoluminescence signals. Quat. Sci. Rev. 11, 33–38.
Duller, G.A.T., 1992. Luminescence Chronology of Raised Marine Terraces, Southwest North Island, New Zealand. University of Wales, Aberystwyth.
Duller, G.A.T., 1994. Luminescence dating of poorly bleached sediments from Scotland. Quat. Sci. Rev. 13, 521–524.
Duller, G.A.T., 2003. Distinguishing quartz and feldspar in single grain luminescence measurements. Radiat. Meas. 37, 161–165.
Duller, G.A.T., 2005. Luminescence Analyst. University of Wales, Aberystwyth.
Duller, G.A.T., 2008. Single-grain optical dating of Quaternary sediments: why aliquot size matters in luminescence dating. Boreas 37, 589–612.
Forman, S.L., Ennis, G., 1992. Limitations of thermoluminescence to date waterlain sediments from glaciated fiord environments of western spitsbergen, svalbard. Quat. Sci. Rev. 11, 61–70.
Fuchs, M., Owen, L.A., 2008. Luminescence dating of glacial and associated sediments: review, recommendations and future directions. Boreas 37, 636–659.
Galbraith, R.F., Laslett, G., 1993. Statistical models for mixed fission track ages. Radiat. Meas. 21, 459–470.
Galbraith, R.F., Roberts, R.G., Laslett, G.M., Yoshida, H., Olley, J.M., 1999. Optical dating of single and multiple grains of quartz from jinmium rock shelter, northern Australia, part 1, Experimental design and statistical models. Archaeometry 41, 339–364.
Gemmell, A.M.D., 1988. Thermo-luminescence dating of glacially transported sediments – some considerations. Quat. Sci. Rev. 7, 277–285.
Holtedahl, O., 1960. Geology of Norway. I Kommisjon Hos H. Aschehoug & Co, Oslo, p. 540.
Holtedahl, O., Dons, J.A., 1960. Geologisk Kart over Norge Berggrunnskart (Geological Map of Norway (Bedrock). Norges Geologiske Undersøkelse Nr. 208, Oslo.
Huntley, D.J., Baril, M.R., 1997. The K content of the K-feldspars being measured in optical dating or in thermoluminescence dating. Anc. TL 15, 11–13.
Hu, G., Zhang, J., Qiu, W., Zhou, L., 2010. Residual OSL signals in modern fluvial sediments from the Yellow River (HuangHe) and the implications for dating young sediments. Quat. Geochronol. 5, 187–193.
Huot, S., Lamothe, M., 2003. Variability of infrared stimulated luminescence properties from fractured feldspar grains. Radiat. Meas. 37, 499–503.
Jaiswal, M.K., Chen, Y.G., Kale, V.S., Achyuthan, H., 2009. Residual luminescence in quartz from slack water deposits in Kaveri basin, south India: a single aliquot approach. Geochronometria 33, 1–8.
King, G.E., Robinson, R.A.J., Finch, A., 2013. Apparent OSL ages of modern deposits from Fåbergstølsdalen, Norway: implications for sampling glacial sediments. J. Quat. Sci. 28, 673–682.
Klasen, N., Fiebig, M., Preusser, F., Radtke, U., 2006. Luminescence properties of glaciofluvial sediments from the Bavarian Alpine Foreland. Radiat. Meas. 41, 866–870.
Klasen, N., Fiebig, M., Preusser, F., Reitner, J.M., Radtke, U., 2007. Luminescence dating of proglacial sediments from the Eastern Alps. Quat. Int. 164–165, 21–32.
Lemon, J., Bolker, B., Oom, S., Klein, E., Rowlingson, B., Wickham, H., Tyagi, A., Eterradossi, O., Grothendieck, G., Toews, M., Kane, J., Turner, R., Witthoft, C., Stander, J., Petzoldt, T., Duursma, R., Biancotto, E., Levy, O., Dutang, C., Solymos, P., Engelmann, R., Hecker, M., Steinbeck, F., Borchers, H., Singmann, H., Toal, T., 2012. Plotrix: Various Plotting Functions.
Matthews, J.A., Olaf Dahl, S., Nesje, A., Berrisford, M.S., Andersson, C., 2000. Holocene glacier variations in central Jotunheimen, southern Norway based on distal glaciolacustrine sediment cores. Quat. Sci. Rev. 19, 1625–1647.
Mejdahl, V., 1979. Thermoluminescence dating: beta-dose attenuation in quartz grains. Archaeometry 21, 61–72.
Mejdahl, V., Funder, S., 1994. Luminescence dating of Late Quaternary sediments from east Greenland. Boreas 23, 525–535.
Miall, A.D., 1985. Architectural-element analysis: a new method of facies analysis applied to fluvial deposits. Earth-Sci. Rev. 22, 261–308.
Murray, A.S., Olley, J.M., Caitcheon, G.G., 1995. Measurement of equivalent doses in quartz from contemporary water-lain sediments using optically stimulated luminescence. Quat. Sci. Rev. 14, 365–371.
Murray, A.S., Wintle, A.G., 2000. Luminescence dating of quartz using an improved single-aliquot regenerative-dose protocol. Radiat. Meas. 32, 57–73.
Murray, A.S., Wintle, A.G., 2003. The single aliquot regenerative dose protocol: potential for improvements in reliability. Radiat. Meas. 37, 377–381.
Murray, A.S., Thomsen, K.J., Masuda, N., Buylaert, J.P., Jain, M., 2012. Identifying well-bleached quartz signals using the different bleaching rates of quartz and feldspar luminescence signals. Radiat. Meas. 47, 688–695.
Nathan, R.P., Thomas, P.J., Jain, M., Murray, A.S., Rhodes, E.J., 2003. Environmental dose rate heterogeneity of beta radiation and its implications for luminescence dating: Monte Carlo modelling and experimental validation. Radiat. Meas. 37, 305–313.
Nesje, A., Kvamme, M., 1991. Holocene glacier and climate variations in western Norway: evidence for early Holocene glacier demise and multiple Neoglacial events. Geology 19, 610–612.
Nesje, A., Kvamme, M., Rye, N., Løvlie, R., 1991. Holocene glacial and climate history of the Jostedalsbreen region, Western Norway; evidence from lake sediments and terrestrial deposits. Quat. Sci. Rev. 10, 87–114.
Nesje, A., Matthews, J.A., Dahl, S.O., Berrisford, M.S., Andersson, C., 2001. Holocene glacier fluctuations of Flatebreen and winter-precipitation changes in the Jostedalsbreen region, western Norvay, based on glaciolacustrine sediment records. Holocene 11, 267–280.
Nesje, A., Olaf Dahl, S., Andersson, C., Matthews, J.A., 2000. The lacustrine sedimentary sequence in Sygneskardvatnet, western Norway: a continuous, high-resolution record of the Jostedalsbreen ice cap during the Holocene. Quat. Sci. Rev. 19, 1047–1065.
Nussbaumer, S.U., Nesje, A., Zumbühl, H.J., 2011. Historical glacier fluctuations of Jostedalsbreen and Folgefonna (southern Norway) reassessed by new pictorial and written evidence. Holocene 21, 455–472.
Odland, A., Røsberg, I., Aarrestad, P.A., Blom, H.H., 1991. Floristic, vegetational and successional patterns on a glacio-fluvial floodplan (sandur) in Jostedal, Western Norway. NINA Forskningsrapp 14, 1–89.
Ollerhead, J., 2001. Light transmittance through dry, sieved sand: some test results. Anc. TL 19, 13–17.
Olley, J., Caitcheon, G., Murray, A., 1998. The distribution of apparent dose as determined by optically stimulated luminescence in small aliquots of fluvial quartz: implications for dating young sediments. Quat. Sci. Rev. 17, 1033–1040.
Østrem, G., Liestøl, O., Wold, B., 1976. Glaciological investigations at nigardsbreen, Norway. Norsk Geografisk Tidsskrift – Nor. J. Geogr. 30, 187–209.
Prescott, J.R., Hutton, J.T., 1994. Cosmic ray contributions to dose rates for luminescence and ESR dating: large depths and long-term time variations. Radiat. Meas. 23, 497–500.
Preusser, F., 1999. Luminescence dating of fluvial sediments and overbank deposits from Gossau, Switzerland: fine grain dating. Quat. Sci. Rev. 18, 217–222.
Readhead, M.L., 2002a. Absorbed dose fraction for ^{87}Rb β particles. Anc. TL 20, 25–28.
Readhead, M.L., 2002b. Addendum to "Absorbed dose fraction for ^{87}Rb β particles". Anc. TL 20, 47.
Reimer, P.J., Baillie, M.G.L., Bard, E., Bayliss, A., Beck, J.W., Blackwell, P.G., Bronk Ramsey, C., Buck, C.E., Burr, G.S., Edwards, R.L., Friedrich, M., Grootes, P.M., Guilderson, T.P., Hajdas, I., Heaton, T.J., Hogg, A.G., Hughen, K.A., Kaiser, K.F., Kromer, B., McCormac, F.G., Manning, S.W., Reimer, R.W., Richards, D.A., Southon, J.R., Talamo, S., Turney, C.S.M., van der Plicht, J., Weyhenmeyer, C.E., 2009. IntCal09 and Marine09 radiocarbon age calibration curves, 0–50,000 years cal BP. Radiocarbon 51, 1111–1150.
Reineck, H.-E., Singh, I.B., 1973. Depositional Sedimentary Environments. Springer-Verlag, Berlin.
Rhodes, E.J., Bailey, R.M., 1997. The effect of thermal transfer on the zeroing of the luminescence of quartz from recent glaciofluvial sediments. Quat. Sci. Rev. 16, 291–298.
Rhodes, E.J., Pownall, L., 1994. Zeroing of the OSL signal in quartz from young glaciofluvial sediments. Radiat. Meas. 23, 581–585.
Rice, S.P., Church, M., 2010. Grain-size sorting within river bars in relation to downstream fining along a wandering channel. Sedimentology 57, 232–251.
Roberts, H.M., Duller, G.A.T., 2004. Standardised growth curves for optical dating of sediment using multiple-grain aliquots. Radiat. Meas. 38, 241–252.
Robinson, R.A.J., Spencer, J.Q.G., Strecker, M.R., Richter, A., Alonso, R.N., 2005. Luminescence dating of alluvial fans in intramontane basins of NW Argentina. Alluvial Fans: geomorphology, Sedimentology. Dynamics 251, 153–168.
RStudio, 2012. RStudio, 0.96.330 ed, Boston, MA.
Sanderson, D.C.W., Bishop, P., Stark, M., Alexander, S., Penny, D., 2007. Luminescence dating of canal sediments from Angkor Borei, Mekong Delta, southern Cambodia. Quat. Geochronol. 2, 322–329.
Shakesby, R.A., Matthews, J.A., Winkler, S., 2004. Glacier variations in Breheimen, southern Norway: relative-age dating of Holocene moraine complexes at six high-altitude glaciers. Holocene 14, 899–910.
Spooner, N.A., 1994. On the optical dating signal from quartz. Radiat. Meas. 23, 593–600.
Stokes, S., Bray, H.E., Blum, M.D., 2001. Optical resetting in large drainage basins: tests of zeroing assumptions using single-aliquot procedures. Quat. Sci. Rev. 20, 879–885.
Telfer, M.W., Bateman, M.D., Carr, A.S., Chase, B.M., 2008. Testing the applicability of a standardized growth curve (SGC) for quartz OSL dating: Kalahari dunes, South African coastal dunes and Florida dune cordons. Quat. Geochronol. 3, 137–142.
Thiel, C., 2011. On the Applicability of Post-IR IRSL Dating to Different Environments, Geowissenschaften. Freien Universitat Berlin, Berlin, p. 186.

Thomsen, K.J., Murray, A.S., Jain, M., Bøtter-Jensen, L., 2008. Laboratory fading rates of various luminescence signals from feldspar-rich sediment extracts. Radiat. Meas. 43, 1474–1486.
Thrasher, I.M., Mauz, B., Chiverrell, R.C., Lang, A., 2009a. Luminescence dating of glaciofluvial deposits: a review. Earth-Sci. Rev. 97, 145–158.
Thrasher, I.M., Mauz, B., Chiverrell, R.C., Lang, A., Thomas, G.S.P., 2009b. Testing an approach to OSL dating of Late Devensian glaciofluvial sediments of the British Isles. J. Quat. Sci. 24, 785–801.
Wallinga, J., 2002. Optically stimulated luminescence dating of fluvial deposits: a review. Boreas 31, 303–322.
Wallinga, J., Bos, A.J.J., Dorenbos, P., Murray, A.S., Schokker, J., 2007. A test case for anomalous fading correction in IRSL dating. Quat. Geochronol. 2, 216–221.
Warnes, G.R., Bolker, B., Bonebakker, L., Gentleman, R., Liaw, W.H.A., Lumley, T., Maechler, M., Magnusson, A., Moeller, S., Schwartz, M., Venables, B., 2010. Gplots: Various R Programming Tools for Plotting data., R Package Version 2.8.0 Ed.